Title
Reaction of gas phase OH with unsaturated self-assembled monolayers and relevance to atmospheric organic oxidations

Journal
Physical Chemistry Chemical Physics, 12(32)

ISSN
1463-9076 1463-9084

Authors
Moussa, Samar G
Finlayson-Pitts, Barbara J

Publication Date
2010

DOI
10.1039/c000447b

Peer reviewed

Reaction of gas phase OH with unsaturated self-assembled monolayers and relevance to atmospheric organic oxidations†

Samar G. Moussa and Barbara J. Finlayson-Pitts*

Received 8th January 2010, Accepted 6th May 2010
DOI: 10.1039/c000447b

The kinetics and mechanisms of the reaction of gas phase OH radicals with organics on surfaces are of fundamental chemical interest, as well as relevant to understanding the degradation of organics on tropospheric surfaces or when they are components of airborne particles. We report here studies of the oxidation of a terminal alkene self-assembled monolayer (7-octenyltrichlorosilane, C8═ SAM) on a germanium attenuated total reflectance crystal by OH radicals at a concentration of 2.1×10^5 cm^{-3} at 1 atm total pressure and 298 K in air. Loss of the reactant SAM and the formation of surface products were followed in real time using infrared spectroscopy. From the rate of loss of the C═C bond, a reaction probability within experimental error of unity was derived. The products formed on the surface include organic nitrates and carbonyl compounds, with yields of $10 \pm 4\%$ and $\leq 7 \pm 4\%$, respectively, and there is evidence for the formation of organic products with C–O bonds such as alcohols, ethers and/or alkyl peroxides and possibly peroxynitrates. The yield of organic nitrates relative to carbonyl compounds is higher than expected based on analogous gas phase mechanisms, suggesting that the branching ratio for the RO_2 + NO reaction is shifted to favor the formation of organic nitrates when the reaction occurs on a surface. Water uptake onto the surface was only slightly enhanced upon oxidation, suggesting that oxidation *per se* cannot be taken as a predictor of increased hydrophilicity of atmospheric organics. These experiments indicate that the mechanisms for the surface reactions are different from gas phase reactions, but the OH oxidation of surface species will still be a significant contributor to determining their lifetimes in air.

Introduction

Surfaces in the Earth's boundary layer are coated with a complex mixture of organic and inorganic compounds that reflect a combination of emissions, uptake onto the surfaces, and degradation by photolysis and interaction with atmospheric oxidants.[1–7] Airborne particles also have a complex composition, with organic compounds as major components.[8–11] The chemistry associated with particles is of major interest because they are known to have adverse impacts on climate, human health and the chemistry of the atmosphere.[8,9,12–14] Aerosols can affect the climate directly through scattering (negative radiative forcing) and absorption (positive radiative forcing) of incoming solar radiation, as well as indirectly through their impact on the properties and lifetimes of clouds. The direct and indirect effects of particles on the climate are responsible for the largest uncertainties in predicting climate change.[14]

Oxidation of organics on surfaces and in or on airborne particles is initiated by reactions with OH, O_3 and NO_3.[13] The kinetics and mechanisms of organic oxidations in the gas phase have been extensively studied and are reasonably well understood,[13,15–18] but much less is known about the reactions of gas phase oxidants with such condensed phase organics. However, there are indications that there are some significant differences compared to reactions in the gas phase. For example, the oxidation reactions tend to be faster than expected based on gas phase kinetics,[19–28] in some cases because of trapping of the oxidants in the organic film which increases the probability of reaction.[29] Reaction mechanisms can also be different. For example, ozonolysis of alkenes on solid substrates forms secondary ozonides (SOZ)[30,31] because the Criegee intermediate and aldehyde or ketone precursors are stabilized and held in sufficiently close proximity to combine, whereas the SOZ yields are negligible under most conditions in the gas phase. Thus, understanding the kinetics and mechanisms of interaction of atmospheric oxidants with condensed phase organics and how they differ from gas phase chemistry is of fundamental chemical interest.

This paper reports studies of the kinetics and mechanisms of reaction of the gas phase OH radical at 1 atm in air with a terminal alkene self-assembled monolayer (SAM) covalently bound to a germanium substrate. The SAM and surface adsorbed products are monitored in real time during the oxidation using infrared spectroscopy, which provides insights into the reaction probability, nature of the products and reaction mechanisms. The implications for the degradation of organics on boundary layer surfaces and in airborne particles are discussed.

Department of Chemistry, University of California, Irvine, California 92697-2025, USA. E-mail: bjfinlay@uci.edu; Fax: +1 949 824 2420; Tel: +1 949 824 7670

† Electronic supplementary information (ESI) available: Detailed description of the reaction cell and calculation of the OH concentration. See DOI: 10.1039/c000447b

Experimental methods

Organic coating

Germanium attenuated total reflectance (ATR) crystals (Pike Technologies, 80 mm × 10 mm × 4 mm) having 10 reflections along the length of the crystal were used. There are relatively few studies in literature regarding the binding of SAMs to germanium compared to silicon,[32–36] but it has been reported that formation of tightly packed and highly oriented monolayers on a Ge surface is less reproducible than those on silicon.[36] This may be due to the instability of the germanium oxide (GeO_2) layer relative to the oxide layer on silicon.[37] Although less is known about SAMs on Ge, the choice of this crystal was based on the much wider spectral range available, down to 860 cm^{-1} in contrast to silicon which has a 1500 cm^{-1} cutoff.

Before use, the crystals were boiled in ethanol and dichloromethane, and then plasma-cleaned (Plasma Cleaner/Sterilizer PDC-32G, Harrick Scientific Products, Inc.) for 30 min at medium power, rinsed with ultrapure water (Milli-Q Plus, 18.2 MΩ cm), and dried in nitrogen (UHP, Oxygen Services Company, 99.999%). The top side of the ATR crystal (area ≈ 3.6 cm^2) was exposed to a 4 mM solution of 7-octenyltrichlorosilane (Sigma-Aldrich, mixture of isomers, 96%, designated throughout as C8═) in hexadecane for 30 min using a custom-made Teflon holder, and then boiled in dichloromethane. The coating was repeated using 10 min exposure time, followed by boiling three times in dichloromethane after which the crystal was wiped using dichloromethane to remove physisorbed residues.[27,31] After coating, the ATR crystal was placed in the reaction cell under a flow of dry nitrogen overnight.

OH generation

Photolysis of isopropyl nitrite (IPN) was used as a source of OH radicals:[17,38–41]

$$(CH_3)_2CHONO + h\nu \rightarrow (CH_3)_2CHO^{\bullet} + NO \quad (1)$$

$$(CH_3)_2CHO^{\bullet} + O_2 \rightarrow CH_3COCH_3 + HO_2 \quad (2)$$

$$HO_2 + NO \rightarrow OH + NO_2 \quad (3)$$

A flow of dry N_2 over liquid IPN (Karl Industries, Ohio) in a glass trap held at 268 K using an ice–salt bath (vapor pressure of IPN at 268 K is 143 Torr)[42] was diluted further with a measured flow of dry air (Scott-Marrin, NO_x < 0.001 ppm, SO_2 < 0.001 ppm, Riverside, CA) to achieve the desired initial concentration of IPN in the gas phase, which ranged from (0.43–17) × 10^{16} molecule cm^{-3}. The IPN concentration was measured by flowing the IPN/N_2/air mixture into a 10.5 cm long cell with quartz windows and recording its UV/visible absorption spectrum (Ocean Optics, Model HR 4000 CG-UV-NIR). The initial IPN concentration was calculated using an absorption cross-section measured in this lab of $\sigma = 1.65 \times 10^{-19}$ cm^2 $molecule^{-1}$ (base e) at 360 nm,[43] which is within 10% of that derived from the spectrum reported by Ludwig and McMillan.[39]

Reaction cell

A custom cell (Fig. 1) described in more detail in the ESI† was designed and constructed for these studies. Briefly, a sealed reaction chamber with quartz end windows is mounted on top of a horizontal ATR holder (Pike Technologies) such that the crystal could be exposed to a gas flow that was simultaneously irradiated to generate OH radicals *via* the IPN photolysis.

After the concentration of IPN was measured, a portion (82–89 cm^3 min^{-1}) of the total flow was diverted to the reaction cell which was located in the sampling compartment of an infrared spectrometer (Mattson Galaxy 5020 FTIR, now Thermo Electron Corp.). The residence time for gases in the cell based on the cell volume (15 cm^3) and flow rate is ~11 s. Background spectra were taken before introducing the IPN/air/N_2 mixture into the cell. Sample spectra (128 scans with a resolution of 4 cm^{-1}) were recorded every 5 min for a period of 30 min in the dark. The lamp was then turned on for 6 h and spectra were collected every 5 min. The lamp used for photolysis was a high pressure Xe arc lamp (Oriel 300 W, Model 6258 OF) equipped with a 10 cm water filter to remove infrared radiation and minimize heating. The depth of penetration of the evanescent wave from the Ge ATR crystal into air was calculated[44] to be 0.13–0.61 μm over the range 4000–860 cm^{-1}, much greater than the thickness of the SAM (~1.3 nm, measured using ellipsometry). The infrared beam thus interrogates the entire organic monolayer and approximates a spectrum similar to a transmission spectrum. All measurements were taken at a total pressure of 1 atm and 298 K.

Ozone generation

Ozone (O_3) was used to completely oxidize the SAM surface. It was generated by irradiating a dry flow of O_2 (UHP; Oxygen Services Company; >99.993%) and He (Oxygen Services Co.; UHP; >99.995%) with a low-pressure mercury lamp (Jelight Company Inc.; Double Bore 78-2046) as described elsewhere.[27,31] The ozone concentration was determined from the absorbance at 254 nm measured in a 30 cm-long cell using $\sigma = 1.15 \times 10^{-17}$ cm^2 $molecule^{-1}$ (base e),[45] and was diluted further with a flow of dry He to obtain the desired concentrations of O_3.

Standards

Calibration for product yield determination was performed by placing small droplets of 2-ethylhexanal (Aldrich, 96%) and 2-ethylhexyl nitrate (Sigma-Aldrich, 97%) on a ZnSe disc (25 × 2 mm, Reflex Analytical Corporation). The disc was immediately analyzed using single beam FTIR transmission spectroscopy (Cygnus 100, Model TR-10001, Mattson Instruments, Inc.) with 128 scans at a resolution of 4 cm^{-1}.

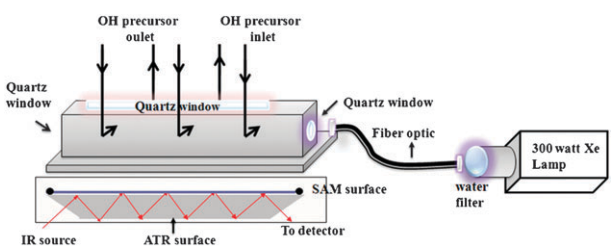

Fig. 1 Schematic diagram of the reaction cell.

The peaks due to C–H stretching in the ~3000–2600 cm^{-1} region were scaled to the same intensity to compensate for differences in volatility and in order to compare directly the absorbances of the nitrate and carbonyl functional groups.

Error analysis

Standard procedures for error analysis[46] were used throughout. Errors are given as $\pm 1s$ (rather than $\pm 1\sigma$), where s is the *sample* standard deviation defined by $s = \sqrt{\frac{\sum_{i=1}^{N}(x_i - \bar{x})^2}{N-1}}$. N represents the number of samples and was between six and eight, depending on the type of measurement. Changes in absorbance with time were used to derive reaction probabilities, product yields and stoichiometry. The absorbances of peaks in an unreacted monolayer are small (<0.01) and the total changes in absorbance due to reaction are typically of the order of 10^{-3}–10^{-4}. As a result, error bars are relatively large. However, within the uncertainties, it will be seen that quantitative analyses can be used to provide insights into the kinetics and mechanisms of the OH–SAM reaction.

Results and discussion

Fig. 2 shows a typical infrared spectrum of the unreacted C8═ SAM on the Ge ATR crystal. The peak at 910 cm^{-1} is due to the out-of-plane deformation of the terminal vinyl group and, as discussed below, is used to follow the loss of double bonds during the reaction. There are also antisymmetric and symmetric stretches of the vinyl group in the 3000–3100 cm^{-1} region; however, these are sufficiently weak that they are not as useful for quantification. The bands at 2925 and 2850 cm^{-1} are due to the $-CH_2-$ antisymmetric (ν_{as}) and symmetric (ν_s) stretches, respectively, and their positions and full widths at half maximum (FWHM) are indicative of order in the monolayer.[47–50] Table 1 compares the positions and FWHM of the $-CH_2-$ stretches for the C8═ SAM on Ge in the present studies to those reported in the literature for well-ordered alkyl SAMs and a less well ordered C8═ SAM on silicon.[27,47,50,51] The SAM in these studies is clearly not as well ordered as alkane SAMS on silicon, which is not

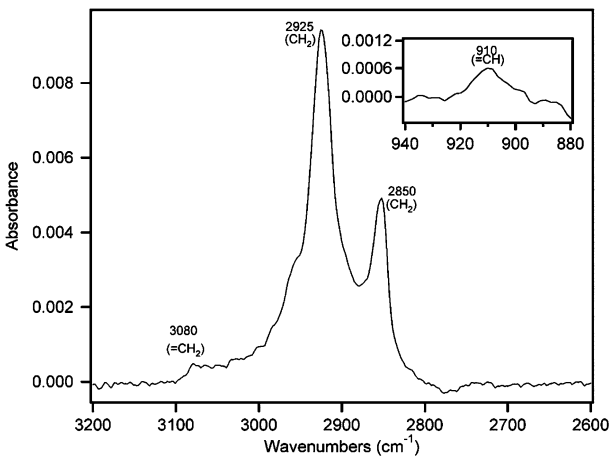

Fig. 2 A typical infrared spectrum of C═ 8 SAM on a germanium ATR crystal.

Table 1 Assignment of the infrared bands for the methylene symmetric and asymmetric stretches and the full width at half maximum (FWHM) for the methylene asymmetric stretch

SAM	ν_{as} (CH_2)/ cm^{-1}	ν_{sy} (CH_2)/ cm^{-1}	FWHM/ cm^{-1}	References
Ordered film	2917	2848	14, 16	50, 47, 51
Less-ordered film	2923	2856	23	27, 51
C8═	2924	2852	30	This study

surprising given the presence of a double bond. The peak positions for $-CH_2-$ in the C8═ SAM on germanium are similar to those on silicon, but the FWHM is significantly larger, indicating a less ordered monolayer than on silicon. This may be due to the greater instability of the oxide layer on Ge.[36,37]

Fig. 3 shows typical spectra as a function of reaction time during exposure to OH. The spectra were obtained by taking the ratio of the single beam of the reacted SAM at different reaction times to the single beam of the unoxidized sample prior to turning on the photolysis lamp; products appear as positive peaks and loss of reactants as negative peaks. Bands due to the vinyl group decreased during the reaction as expected for reaction of OH with the double bond. However, the intensities of the bands due to $-CH_2-$ also decreased significantly. Two strong absorption bands at 1634 and 1280 cm^{-1} indicate the formation of organic nitrates ($-ONO_2$).[52] A broad peak at 1726 cm^{-1} is in the region expected for aldehydes and ketones.[52] Peroxynitrates, $ROONO_2$, also have a characteristic $-NO_2$ asymmetric stretch in this region as well as a symmetric stretch around 1300 cm^{-1} and an N–O stretch around 790 cm^{-1}. However, observation of these latter two bands, if they are present, was precluded by overlap with the strong nitrate peak at 1280 cm^{-1} and the cutoff of the Ge crystal at 865 cm^{-1}, respectively. As discussed below, the formation of C═O on the surface is expected mechanistically, but a contribution from peroxynitrates is possible as well. Broad peaks at 1434 and 1370 cm^{-1} are assigned to nitrate ions; NO_2 is generated

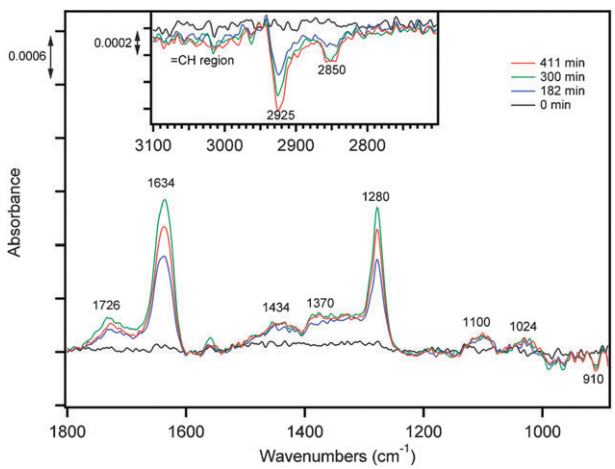

Fig. 3 ATR spectra of C8═ SAM upon exposure to OH formed by the photolysis of ~1 × 10^{17} molecule cm^{-3} of IPN. The y axis is the $\log_{10}(S_0/S_1)$, where S_0 is single beam spectrum of the unreacted SAM and S_1 is the single beam spectrum of the reacted SAM at increasing reaction times.

in the photolysis and secondary chemistry of isopropyl nitrite, and the OH + NO_2 reaction generates HNO_3, some of which is taken up by the surface and dissociates. Similar peaks were seen when an unreacted SAM was exposed to gaseous HNO_3 in the presence of water vapor. Finally, peaks of variable relative intensities around 1024 and 1100 cm^{-1} characteristic of a C–O stretch, *e.g.*, in an alcohol, ether or alkyl peroxide,[52] were sufficiently weak that they were not always detectable. If due to an alcohol, an accompanying strong peak in the 3500 cm^{-1} region due to the O–H stretch would also be expected. As discussed below, alcohols will be formed by addition of OH to the double bond, yet such a feature due to the O–H stretch was not present in our spectra, nor in those of previous studies of alcohol–SAMs.[53,54] For example, even in the infrared spectrum of a monolayer of 16-mercapto-hexadecane-1-ol on Au in which all the chains have –OH terminal groups, only the $–CH_2–$ stretches and the C–O stretch at 1070 cm^{-1} were observed.[54] Thus, although alcohols are expected to be major products of the reaction, they are not necessarily readily observable by ATR-FTIR.

Fig. 4 shows the time dependence in a typical experiment for the peaks at 1726, 1634 and 1280 cm^{-1}, as well as those due to the reactant vinyl and $–CH_2–$ groups. It is clear from Fig. 4 that not all of the double bonds have reacted after 400 minutes, while products continue to be generated. This is in contrast to previous studies of the ozonolysis of alkene SAMs in which complete reaction of the monolayer was manifested with no further changes in the vinyl peak intensities after ~10 min of reaction with ~10^{14} O_3 cm^{-3}.[27,31] The fraction of C=C loss due to the OH reaction in the present studies was determined using the absorbance relative to that of a fully oxidized monolayer obtained by further exposing the OH oxidized film to ozone. Fig. 5 shows the intensity of the vinyl peak at 910 cm^{-1} as a function of time during a typical OH exposure, and after further reaction with O_3. The plateau region reached

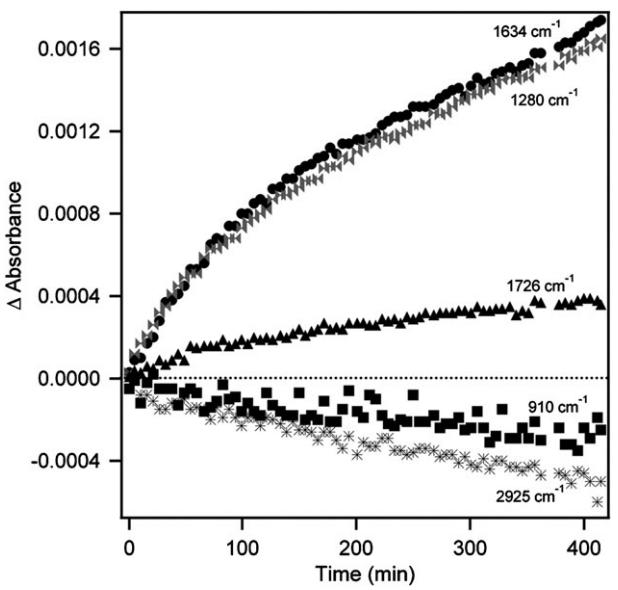

Fig. 4 Changes in absorbance as a function of time for selected bands during a typical reaction of C8= SAM with OH using an initial IPN concentration of 1.6 × 10^{17} molecule cm^{-3}.

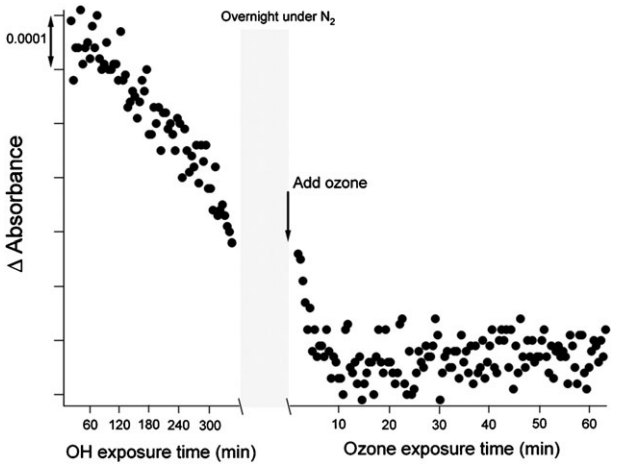

Fig. 5 Changes in the absorbance of C=C at 910 cm^{-1} after exposure to OH ($[IPN]_0$ = 1.6 × 10^{17} molecule cm^{-3}), held in a flow of dry N_2 overnight and then reacted with 4.8 × 10^{13} O_3 per cm^3. No change in the C=C peak occurred while the sample was under a flow of N_2 overnight. The C=C is completely reacted after ~8 minutes of ozonolysis.

after ozonolysis represents full oxidation of the C=C in the SAM. Using this approach, the average loss of the C=C group in the eight experiments reported here was calculated to be 37 ± 18%. This approach also provided the data needed to calculate the reaction probability for OH with the SAM, as discussed in the following section.

Kinetics

From conventional gas kinetic molecular theory, the number of reactions per cm^2 per second between a gas and a surface in the absence of diffusion limitations is given by eqn (I):

$$\frac{d\{C=C\}}{dt} = \text{No. of reactions per cm}^2\text{ per s} = [OH]\gamma\sqrt{\frac{RT}{2\pi M}} \quad \text{(I)}$$

where M is the molecular mass of the hydroxyl radical present at concentration [OH] in the gas phase, R is the gas constant, T is the temperature (K) and γ is the reaction probability, *i.e.* the fraction of collisions of OH with the surface that lead to reaction. The rate of the surface reaction is measured here as the rate of loss of C=C from the surface monolayer. From the Beer–Lambert law, the number of C=C on the surface per cm^2 at time t, $\{C=C\}_t$, is given by eqn (II),

$$\frac{\{C=C\}_t}{\{C=C\}_\infty} = \frac{\text{abs}(C=C)_t}{\text{abs}(C=C)_\infty} \quad \text{(II)}$$

where $\{C=C\}_\infty$ is the total loss of C=C per cm^2 at complete reaction of the monolayer, and "abs" indicates the corresponding absorbances at time t and $t = \infty$, respectively. The latter is obtained from the net change in the absorbance after complete reaction of the monolayer with OH and then O_3 (Fig. 5). In a fully oxidized SAM, the total change in the surface density of C=C, *i.e.*, $\{C=C\}_\infty$, is assumed to be equal

to the initial SAM density, *i.e.* $[SAM]_0$. The rate of change of the C=C bonds per cm^2 on the surface is thus given by:

$$\frac{d\{C=C\}}{dt} = \frac{d[abs(C=C)]}{dt}\frac{[SAM]_0}{abs(C=C)_\infty} \qquad (III)$$

The surface density of a monolayer on germanium is not well known. Maoz and Sagiv[36] reported that the absorbance per $-CH_2-$ group per ATR reflection on germanium is 1.4×10^{-4}, and that on silicon is 2.1×10^{-4}. This suggests that a monolayer on Ge is not as densely packed as on Si. Taking the monolayer surface density of a C8 alkane SAM on Si as 4.2×10^{14} molecules cm^{-2},[55,56] the Maoz and Sagiv data for $-CH_2-$ indicate that the average surface density of a monolayer on germanium is 2.8×10^{14} molecules cm^{-2}. However, the variability in the surface density of SAMs on germanium[36] is such that a single average value cannot be taken for all runs. As a result, for each experiment, the measured absorbance at 2925 cm^{-1} prior to exposure to OH was used to calculate $[SAM]_0$ in these experiments.

The left side of eqn (III) gives the number of SAM C=C groups reacting per cm^2 per second. In order to obtain the reaction probability (γ) from eqn (I), the concentration of OH impinging on the surface must be known. Details of how the OH concentrations were derived are given in the ESI.† In brief, the rate of decay of IPN in the photolyzing light beam was measured in separate experiments using its absorption at 360 nm. Decay of IPN in this system is primarily due to photolysis and reaction of the OH generated in reactions (1)–(3). A model for chemistry in this system that consisted of 111 gas phase reactions was developed and the photolysis rate constant, k_p, for IPN was obtained by varying it to obtain a best fit to the experimentally measured decay. (A full model rather than just reactions (1)–(3) takes into account other loss processes for OH in this system, which is important in calculating its concentrations. In addition, the model predicts the formation of products such as HNO_3 that contribute to the surface product spectra and to gaseous species such as NO_2 that can participate in the secondary chemistry.) However, in order to minimize direct photochemistry on the surface and for geometric reasons, the SAM-coated surface is located below the quartz end windows (Fig. 1) and hence is not exposed directly to the incoming light beam. Because of the short lifetime of OH with respect to IPN ($\tau < 0.6$ ms), the OH generated in the beam itself does not reach the SAM, and consequently it is the concentration of OH generated by IPN photolysis due to scattered light in the cell directly above and at the crystal surface that is available for reaction. In order to obtain the effective OH concentration at the surface, the value of k_p measured directly in the lamp beam was scaled by the light intensity measured in separate experiments at the position of the crystal surface compared to that passing directly through the center of the cell. The average OH concentration obtained using this approach was 2.1×10^5 OH radicals cm^{-3}.

Table 2 summarizes the reaction probabilities obtained using this OH concentration and eqn (I)–(III). Given the small peak intensities for a monolayer, the rate of loss had to be measured over a large extent of reaction, averaging 37% loss of the C=C bonds. The reaction probability derived, $\gamma = 1.1 \pm 0.9$, thus represents an average value. Diffusion corrections were not applied since the OH is largely generated essentially at the surface; in addition any such corrections will be well within the error bars of the measurements. However, the ratio of the increase in the $-ONO_2$ peaks at 1634 and 1280 cm^{-1} to the decrease in the C=C at 910 cm^{-1} was constant with time, indicating that the reaction probability did not change significantly over our reaction times. The major sources of uncertainty are in the OH concentration at the surface of the crystal, which is dominated by uncertainties in the light intensity at the surface, as well as uncertainties in the initial SAM concentration and the rates of C=C decay.

Within experimental error, reaction occurs on essentially every collision. In the gas phase, the reaction of OH with longer chain terminal alkenes occurs with rate constants of the order of 4×10^{-11} cm^3 $molecule^{-1}$ s^{-1}, which corresponds to reaction in approximately every 5 collisions. An enhanced reaction probability for the surface reaction is consistent with the fact that the terminal double bond should be the part of the SAM that OH first encounters in the structured monolayer, as also proposed for the NO_3 reaction,[57] and with previous studies showing enhanced reactivity at interfaces compared to the gas phase.[19–28] Reaction on every collision has also been observed for the reaction of Cl atoms with a C3= SAM.[22]

Although there are a number of studies of the OH oxidation of organics on surfaces and in or on particles, there are

Table 2 Summary of decay rates for C=C and $-CH_2-$ groups[a] and reaction probabilities for OH reacting with a C8= SAM at 298 K and 1 atm pressure in air

Experiment	$[IPN]_0$ (10^{16} molecule cm^{-3})	$[SAM]_0$ (10^{14} molecule cm^{-2})	γ	10^8 Rate (s^{-1}) (2925 cm^{-1})	10^8 Rate (s^{-1}) (910 cm^{-1})	$\Delta CH_2/\Delta C=C$
1	17	3.0	2.7 ± 4.4	2.5	1.8	0.67
2	16	2.0	1.0 ± 1.7	1.8	0.96	0.88
3	9.5	1.4	0.6 ± 1.1	2.6	0.94	1.3
4	3.5	1.5	0.5 ± 0.8	1.7	0.62	1.3
5	4.6	2.1	1.5 ± 2.5	2.2	1.1	0.98
6	3.0	3.1	1.8 ± 3.0	3.0	1.7	0.86
7	0.68	1.9	0.1 ± 0.2	0.09	0.06	2.1
8	0.43	1.9	0.5 ± 0.9	1.5	0.35	0.71
Average (±1s)			**1.1 ± 0.9**			**1.1 ± 0.5**

[a] The 910 cm^{-1} band is used for C=C and the 2925 cm^{-1} band for $-CH_2-$. The average OH concentration was 2.1×10^5 molecules cm^{-3}. [b] Rate of decay of the individual absorbance peaks.

relatively few involving SAMs. Bertram *et al.*[25] measured reaction probabilities for OH with a C3═ SAM in the range from 0.25–1, with an average of 0.6, in excellent agreement with our results for the C8═ SAM. Molina *et al.*[26] reported $\gamma > 0.2$ for the OH reaction with a C18 alkane monolayer, and Bertram *et al.*[25] measured $\gamma = 0.29$ for the same surface, indicating that even for saturated alkyl chains, the surface reaction is fast. In the studies of D'Andrea *et al.*[53] of OH with a terminal alkene thiol SAM on gold, most of the C═C had reacted after 5 minutes.

Product yields

Data such as those in Fig. 3 and 4 can be used to determine some of the product yields as well as the loss of organic material from the surface. It is clear that the organic nitrate peaks at 1634 and 1280 cm^{-1} are intense relative to the peak at 1726 cm^{-1}; we assume here that the latter is due solely to C═O, although as discussed above, there may be some contribution from peroxynitrates. The very weak absorbances of the peaks in the C–O stretching region and the lack of specific identification of the species responsible preclude their quantification.

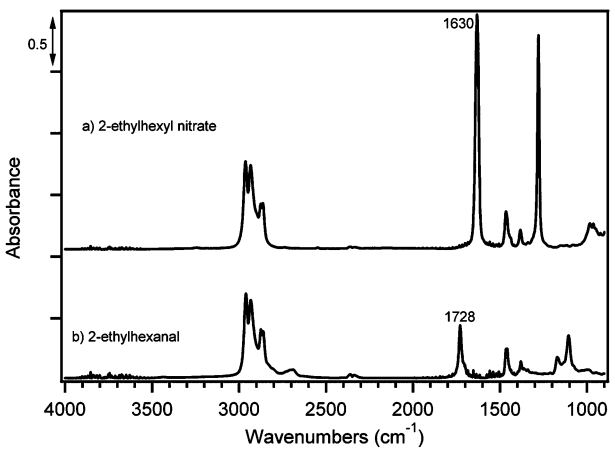

Fig. 6 Transmission spectra of (a) 2-ethylhexyl nitrate and (b) 2-ethylhexanal on a ZnSe window. The *y* axis is the $\log_{10}(S_0/S_1)$ where S_0 is single beam spectrum of the bare ZnSe window and S_1 is the single beam spectrum of the different compounds.

The differences in relative intensities of the absorption bands may be due to different infrared absorption cross-sections for $-ONO_2$ compared to C═O. In order to address this issue, transmission spectra were recorded for 2-ethylhexanal and 2-ethylhexyl nitrate (Fig. 6). Product yields were obtained by using the spectra in Fig. 6 to obtain the relative absorbance of the 1630 cm^{-1} organic nitrate band and the C–H stretches by integrating over each of these regions and taking the ratio. For the calibration compounds, there are 17 alkyl C–H bonds in the organic nitrate and 15 alkyl C–H bonds in the aldehyde. The ratio of the $-ONO_2$ peak area at 1630 cm^{-1} to the total area for the C–H peaks for the calibration compounds was measured from the data in Fig. 6 and then knowing the number of C–H bonds in each compound, the ratio for one $-ONO_2$ peak per C–H group was determined. Based on the presence of 12 alkyl C–H bonds in the unreacted SAM, the expected ratio of the absorbance at 1630 cm^{-1} to that in the C–H stretching region that corresponds to one $-ONO_2$ peak per C8═ SAM could be calculated. This was taken as an equivalent monolayer of organic nitrate.

For each experiment, the ratio of the 1630 cm^{-1} peak during the reaction to the C–H peaks before reaction was then used to obtain the fraction of a monolayer that contains organic nitrate groups as a function of reaction time. Since as described earlier, the initial surface density of the SAM is measured for each experiment, this gives the absolute number of $-ONO_2$ groups per cm^2 formed as a function of reaction time. As described above in the kinetics section, the loss of C═C group per cm^2 can also be determined as a function of reaction time using the 910 cm^{-1} peak. A plot of the formation of $-ONO_2$ against the loss of C═C gives the number of organic nitrate products on the surface formed per reaction of C═C, *i.e.*, the product yield. Table 3 shows that the average yield of organic nitrates on the surface is 10 ± 4%. A similar approach for C═O gives a yield of (aldehydes + ketones) on the surface of 7 ± 4%; this will be an upper limit if $ROONO_2$ products contribute to the 1726 cm^{-1} peak as well. The calculation of these yields assumes that the relative intensities of the $-ONO_2$ and –C═O functional groups in the liquid films used as calibrations also apply to the SAMs. It is emphasized that these represent product yields of surface species only (gas phase species could not be detected), and do not include the alcohols, ethers or organic peroxides that are responsible

Table 3 Extent of loss of C═C and product yields for organic nitrates and carbonyl compounds after 6 hours of reaction

Experiment	$[IPN]_0$ (10^{16} molecule cm^{-3})	$[SAM]_0$ (10^{14} molecule cm^{-2})	% Loss of C═C[a]	% Yield $RONO_2$	% Yield RC═O
1	17	3.0	63	8.4	12
2	16	2.0	42	12	6.6
3	9.5	1.4	35	17	14
4	3.5	1.5	28	6.8	2.7
5	4.6	2.1	56	8.0	4.9
6	3.0	3.1	44	8.9	4.2
7	0.68	1.9	8.0	[c]	[c]
8	0.43	1.9	23	[c]	[c]
Average (±1*s*)			**37 ± 18**	**10 ± 4**	**7 ± 4**

[a] Based on the fraction of the 910 cm^{-1} peak that is lost after 6 hours reaction time, complete reaction of the vinyl group is obtained from the net decrease in the peak after reaction with O_3; see text. [b] Yields defined as the number of each functional group formed per C═C reacted; see text. [c] Peaks too small to quantify reliably.

for peaks in the 1000–1200 cm^{-1} region or other weak peaks that are not observable by ATR-FTIR.

Mechanism

The initial reaction is expected to be primarily OH addition to the double bond to form a β-hydroxyalkyl radical (Scheme 1).[13,15–18] The second step is the transformation of the alkyl radical to a β-hydroxyalkylperoxy radical which can react with NO_2 (from the IPN photolysis and secondary chemistry) to form a peroxynitrate. In the presence of NO, the alkylperoxy radical can also be converted to a surface alkyl nitrate, consistent with the increase in the 1634 cm^{-1} and 1280 cm^{-1} peaks. In the gas phase, the major pathway for reaction of an alkylperoxy radical with NO leads to the formation of a β-hydroxyalkoxy radical which isomerizes or decomposes (reaction with O_2 is relatively slow for these radicals).[58] Matsunaga *et al.*[59] report that the gas phase oxidation of terminal alkenes by OH in the presence of NO_x ultimately forms cyclic hemiacetals and dihydrofurans *via* a mechanism involving reverse isomerization. If an analogous mechanism was applied here and these compounds were major products, there should be strong, characteristic absorption bands[52,60,61] at ~1060 and 1150 cm^{-1}. However, these were not observed, indicating that the mechanism for SAM oxidation on a surface does not follow that for the gas phase, at least in this respect.

A key difference between the gas phase and surface reactions is the surrounding milieu of closely packed hydrocarbon chains in the SAM. This makes isomerization through a 1,5 H-shift involving a 6-membered ring transition state less likely than in the gas phase where the hydrocarbon backbone is flexible and does not have nearest neighbors. This difference has been manifested in free radical reactions between adjacent chains in other studies. For example, Wu *et al.*[62,63] reported the formation of epoxides and hydroxyepoxides in the autoxidation of unsaturated fatty acids adsorbed to silica gel. This was attributed to the addition of RO_2 on one chain to the double bond on an adjacent chain, and to a competing hydrogen abstraction by RO_2, both of which are known to occur in the condensed phase.[64] Such reactions in the SAM could lead to the formation of epoxides and peroxides, cross-linking of the chains, and may be responsible for the weak infrared bands in the 1000–1200 cm^{-1} region.

Direct abstraction by OH from the alkyl chain, especially at the allylic position, is another potential reaction path that has been reported to be a minor, but not insignificant, path in the gas phase oxidation of linear alkenes.[13,40] In the SAMs, the double bond is located at the chain terminus where gas phase OH first interacts with the organic, which would be expected to enhance addition compared to abstraction. Enhanced reactivity due to the presence of a double bond at the interface has also been reported for the NO_3 reaction with a terminal

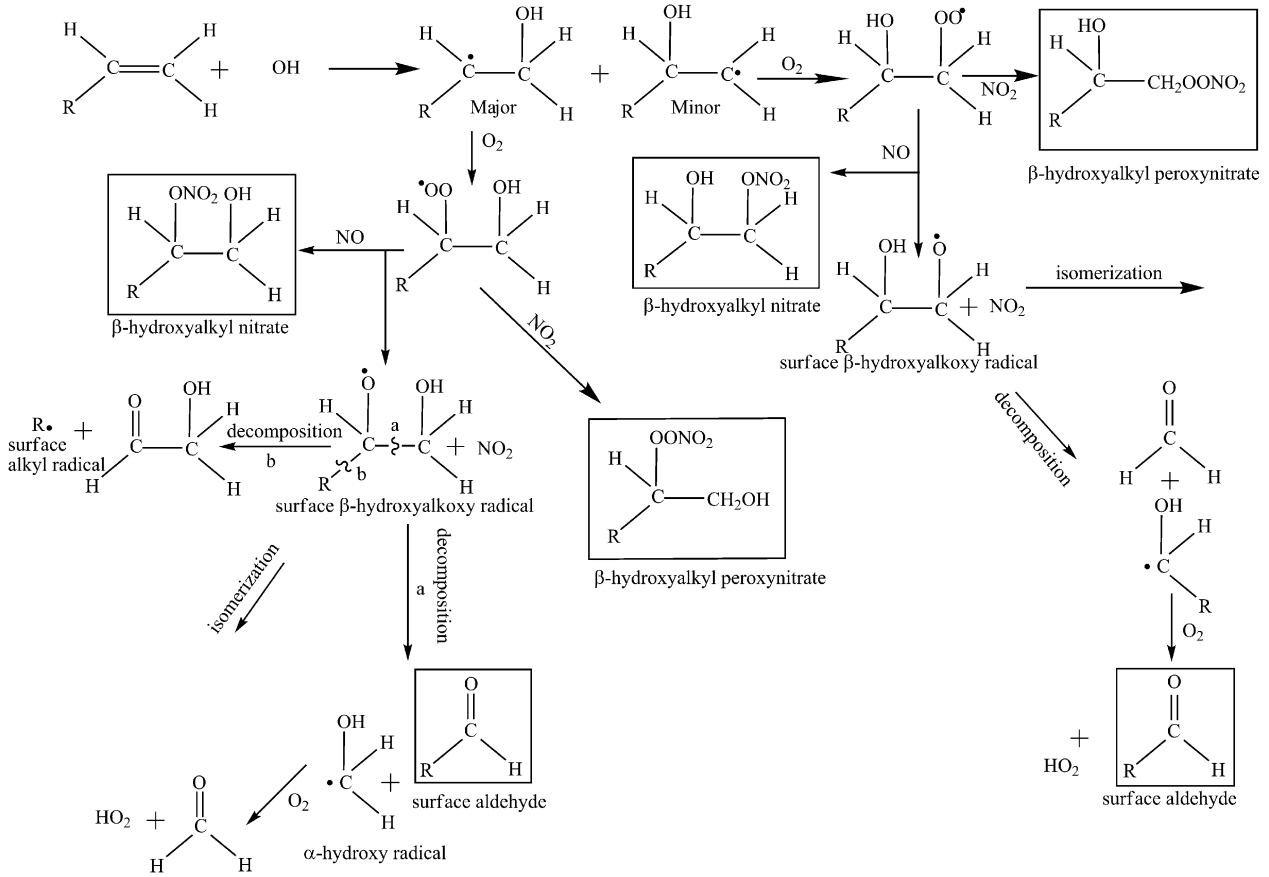

Scheme 1 Partial mechanism for the reaction of C8═ SAM with OH leading to the observed –ONO_2 and –C═O functionalities. The molecules in the boxes are surface products. As discussed in the text, the isomerization pathway for the surface β-hydroxyalkoxy radical which is important in the gas phase does not appear to be significant in this system, and there are a number of additional products which could not be quantified.

alkene SAM.[57] In the present experiments, a C8 alkane SAM on Ge was exposed to OH under the same conditions as for the C8═ SAM, but negligible amounts of reaction occurred. D'Andrea *et al.*[53] studied the reaction of OH with a terminal alkene SAM on gold, Au/HS$(CH_2)_9CH{=}CH_2$, and observed that when most of the C═C had reacted, the alkyl chain was intact, consistent with addition to the terminal double bond being the major reaction pathway; however, these experiments were carried out at low pressures in the absence of O_2.

The yield of organic nitrates in these studies, 10 ± 4%, can be compared to yields measured from the gas phase OH oxidation of alkenes in the presence of NO. For example, Matsunaga and Ziemann[40] measured a 14% yield of nitrates from the addition path. When both addition and abstraction were taken into account, the overall yield was 9%. Although this yield is for particle nitrates, it should represent the total nitrate yield since the high molecular weights of the reactants and products will favor partitioning into the condensed phase.

It is noteworthy that the yields of organic nitrates and carbonyl products on the surface are similar (Table 3). In the gas phase, the formation of organic nitrates from the RO_2 + NO reaction represents a minor pathway (<30%)[40,65] compared to the generation of RO + NO_2. As seen in Scheme 1, the latter branch should form surface aldehydes so that one might have anticipated by analogy to gas phase chemistry that the surface carbonyl yield would be significantly larger than that of the organic nitrates. The larger yield of organic nitrates in the present studies relative to carbonyl yields may reflect enhanced stabilization of the (ROO–NO)[66] intermediates that form $RONO_2$ due to the densely packed monolayer. Alternatively, the packing of the monolayer may yield RO_2 radicals with structures that favor the *trans*-form of ROO–NO over the *cis*-, where the *trans* form has been proposed to be responsible for organic nitrate formation.[66]

A significant decrease in the peaks at 2925 and 2850 cm^{-1} due to $–CH_2–$ groups is also observed. From spectra such as those in Fig. 2, the average ratio of the net absorbance of the 2925 cm^{-1} peak to that at 910 cm^{-1} was measured to be 12.5 ± 5.5 for the unreacted C8═ SAM. This represents six $–CH_2–$ groups and one C═C group. The corresponding ratio of average peak intensities for one CH_2 group per C═C is therefore 12.5/6 or 2.1 ± 0.9. The ratios of the rates of decay of the 2925 cm^{-1} and 910 cm^{-1} bands summarized in Table 2 were used with this relationship for the relative intensities of the peaks to calculate the change in the number of $–CH_2–$ groups detected relative to C═C in each run. An average change of (1.1 ± 0.5) $–CH_2–$ groups per C═C is obtained (Table 2).

There are a number of potential reasons for this decrease in the $–CH_2–$ signal. First, oxidation may disrupt the film morphology in such a way that $–CH_2–$ groups are moved away from the crystal surface so that they are no longer fully interrogated by the infrared beam. The absorption intensity is also sensitive to the orientation of the $–CH_2–$ groups relative to the surface normal so that disordering can lead to changes in the detected signal. While this has been proposed in studies of SAM oxidations by Cl atoms and NO_3 radicals,[22,57] SAMs on Ge initially are not as ordered as conventional SAMs on silicon or gold (Table 1) so it is not clear whether this is a major factor in the present case. Finally, chain scission with loss of organics to the gas phase can occur *via* secondary chemistry involving free radical reactions induced by initial addition of OH to the double bond, with potentially minor contributions from direct abstraction. As discussed earlier, reactions between free radicals on one chain with an adjacent one are likely to occur, leading to bond scission and release of gas phase products with the number of carbons released depending on the site of attack on the second chain. Molina *et al.*[26] reported that an octadecyltrichlorosilane, (C18) alkane SAM, was essentially completely removed by reaction with ~10^8 OH cm^{-3} for only 10 min, and Moise and Rudich[22] reported 20% loss of carbon during the reaction of chlorine atoms with SAMs. Vlasenko *et al.*[67] reported the production of significant amounts of gas phase products from the OH oxidation of a stearic acid film due to bond scission after attack of OH on the chain.

Water adsorption on oxidized SAMs

It is commonly expected that oxidation of hydrophobic organics such as the C8═ SAM will increase hydrophilicity and water uptake.[22] Fig. 7 shows a typical infrared spectrum of the SAM exposed to water vapor at relative humidities between 20 and 80% prior to (Fig. 7a), and after oxidation with OH (Fig. 7b) and then with ozone (Fig. 7c). The absorbance spectra are generated by taking the ratio of the single beam after exposing the surface to water to that of the dry sample. There appears to be a slight enhancement of water uptake upon oxidation. In addition, the shoulder at 3200 cm^{-1} that is characteristic of

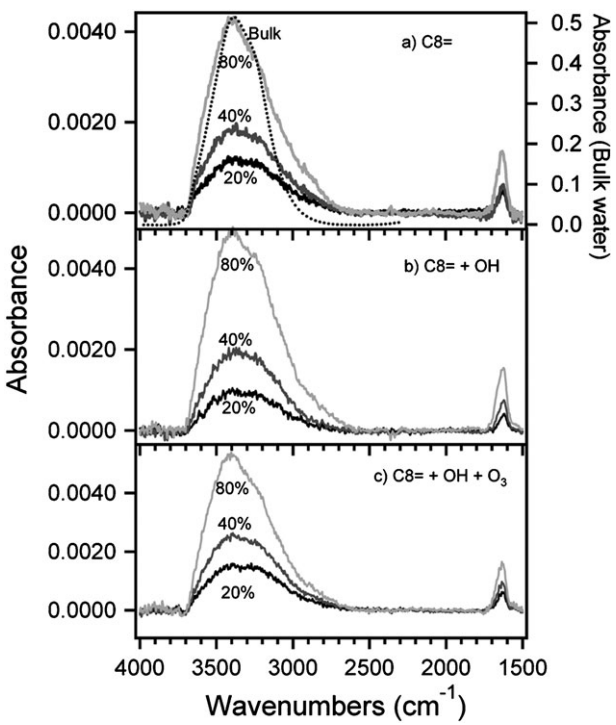

Fig. 7 Infrared spectra of adsorbed water in equilibrium with water vapor at different relative humidities for a Ge ATR crystal coated with (a) C8═ SAM, (b) C8═ SAM exposed to OH for 6 hours, (c) C8═ SAMs exposed to both OH and O_3. The dotted line in (a) is the spectrum of bulk liquid water.

structured water on the surface is slightly more pronounced in the oxidized surface. This is similar to our previous results[51,68] where oxidation of the film using O_3 or $KMnO_4$ only slightly enhanced the uptake of water. Possible reasons for this are hydrogen-bonding between polar groups on the surface so they are not available for interaction with water[51,69–71] or the polar groups being buried inside the organic surface film in such a way that they are not available for interaction with the gas phase.[72]

Conclusions and atmospheric implications

The reaction of OH radicals with a terminal alkene self-assembled monolayer is fast, with a reaction probability indistinguishable from unity. Organic nitrates and (aldehydes + ketones) are the major functional groups identified on the surface, and in comparable amounts, which is surprising. The intermediates formed in the RO_2 + NO reaction that isomerize to generate $RONO_2$ may be preferentially stabilized relative to the formation of RO + NO_2 when the reaction occurs on a surface, or the *trans* form of the ROONO intermediate that leads to $RONO_2$ may be favored on the surface. Thus, organic nitrates may be larger contributors to the products of oxidation of surface films and airborne particles than expected based on analogies to gas phase chemistry. There is also evidence for the formation of products containing C–O functionalities such as alcohols, and possibly peroxynitrates, which given the measured yields of surface nitrates and carbonyls must represent the majority of the products. Despite the formation of such products, uptake of water did not increase substantially. The nature and yields of the products formed indicate that the mechanism does not closely follow that for gas phase reactions, which has also been reported for oxidation of organics in particles, *e.g.*, by NO_3 and Cl atoms.[57,73,74]

The concentration of OH used in these studies, 2.1×10^5 radicals cm^{-3}, is actually about one to two orders of magnitude smaller than encountered mid-day in the troposphere.[13] Given a reaction probability of unity, the half-life of the C=C group would only be 0.09–0.9 hours for typical mid-day OH concentrations of 2×10^6 to 2×10^7 radicals cm^{-3} in air. For comparison, the lifetime of an alkene SAM on silica with respect to reaction with 80 ppb O_3 was estimated to be $\sim$0.6 h.[27] Gross and Bertram[57] recently reported a reaction probability for a terminal alkene SAM of $\gamma = 0.034$ with the NO_3 radical, which would give a comparable range of lifetimes to those for the OH reaction at NO_3 radical concentrations in the range from 2.5–25 ppt (although this would be operative at night while OH is primarily a daytime process). While urban organic surface films are expected to consist largely of saturated organics rather than alkenes as studied here,[1–7] the reaction probabilities for OH with alkyl groups have also been shown to be large.[25,26,53] Given the production of gas phase products in both the alkene and alkane reactions, the OH reaction is expected to provide an efficient mechanism for removing organics from urban surfaces and generating gas phase oxidized products. The SAMs studied here are structurally different from organics in airborne particles and hence simple extrapolation of these results to oxidation of atmospheric aerosols should be approached with caution. However, a number of studies of the reactions of OH with aerosols comprised of organics such as bis(2-ethylhexyl)sebacate, *n*-hexacosane, squalane, motor oil, palmitic acid, stearic acid and sodium oleate as models of SOA have been carried out.[67,75–82] As reported for the OH reaction with alkane SAMs,[25,26] the reactions are fast and conversion of some of the particle mass to gas phase products has also been observed.

Acknowledgements

We are grateful to the National Science Foundation (CHE 0431312 and CHE 0909227) for support of this work. We also thank Ron Hulme and Lee Moritz in the machine shop for their help in the design and construction of the photolysis cell, and Jörg Meyer for technical assistance. We also would like to thank Jonathan Raff, Theresa McIntire, Allie Margarella, John Hemminger, Vu Phan, Veronique Perraud, Emily Bruns, Stan Johnson and James N. Pitts Jr. for helpful discussions and technical assistance. SGM thanks the Air & Waste Management Association (AWMA) for a scholarship and the Michael E. Gebel Award Fund for partial financial support.

References

1 M. L. Diamond, S. E. Gingrich, K. Fertuck, B. E. McCarry, G. A. Stern, B. Billeck, B. Grift, D. Brooker and T. D. Yager, *Environ. Sci. Technol.*, 2000, **34**, 2900–2908.
2 S. E. Gingrich and M. L. Diamond, *Environ. Sci. Technol.*, 2001, **35**, 4031–4037.
3 B. Lam, M. L. Diamond, A. J. Simpson, P. A. Makar, J. Truong and N. A. Hernandez-Martinez, *Atmos. Environ.*, 2005, **39**, 6578–6586.
4 N. L. Law and M. L. Diamond, *Chemosphere*, 1998, **36**, 2607–2620.
5 Q. T. Liu, R. Chen, B. E. McCarry, M. L. Diamond and B. Bahavar, *Environ. Sci. Technol.*, 2003, **37**, 2340–2349.
6 Q. T. Liu, M. L. Diamond, S. E. Gingrich, J. M. Ondov, P. Maciejczyk and G. A. Stern, *Environ. Pollut.*, 2003, **122**, 51–61.
7 A. J. Simpson, B. Lam, M. L. Diamond, D. J. Donaldson, B. A. Lefebvre, A. Q. Moser, A. J. Williams, N. I. Larin and M. P. Kvasha, *Chemosphere*, 2006, **63**, 142–152.
8 Y. Rudich, *Chem. Rev.*, 2003, **103**, 5097–5124.
9 Y. Rudich, N. M. Donahue and T. F. Mentel, *Annu. Rev. Phys. Chem.*, 2007, **58**, 321–352.
10 J. H. Kroll and J. H. Seinfeld, *Atmos. Environ.*, 2008, **42**, 3593–3624.
11 M. Hallquist, J. C. Wenger, U. Baltensperger, Y. Rudich, D. Simpson, M. Claeys, J. Dommen, N. M. Donahue, C. George, A. H. Goldstein, J. F. Hamilton, H. Herrmann, T. Hoffmann, Y. Iinuma, M. Jang, M. E. Jenkin, J. L. Jimenez, A. Kiendler-Scharr, W. Maenhaut, G. McFiggans, T. F. Mentel, A. Monod, A. S. H. Prevot, J. H. Seinfeld, J. D. Surratt, R. Szmigielski and J. Wildt, *Atmos. Chem. Phys.*, 2009, **9**, 5155–5236.
12 B. J. Finlayson-Pitts, *Phys. Chem. Chem. Phys.*, 2009, **11**, 7760–7779.
13 B. J. Finlayson-Pitts and J. N. Pitts, Jr., *Chemistry of the Upper and Lower Atmosphere: Theory, Experiments and Applications*, Academic Press, San Diego, 2000.
14 Intergovernmental Panel on Climate Change, Climate Change 2007: The Physical Science Basis Summary for Policy Makers, Intergovernmental Panel on Climate Change, 2007.
15 R. Atkinson, *J. Phys. Chem. Ref. Data*, 1994, R1.
16 R. Atkinson, *J. Phys. Chem. Ref. Data*, 1997, **26**, 215–290.
17 R. Atkinson, *Pure Appl. Chem.*, 1998, **70**, 1335–1343.
18 R. Atkinson, *Atmos. Environ.*, 2000, **34**, 2063–2101.
19 C. C. Lai, S. Yang and B. J. Finlayson-Pitts, *Langmuir*, 1994, **10**, 4637–4644.
20 B. T. Mmereki and D. J. Donaldson, *J. Phys. Chem. A*, 2003, **107**, 11038–11042.

21 T. Moise and Y. Rudich, *J. Geophys. Res., [Atmos.]*, 2000, **105**, 14667–14676.
22 T. Moise and Y. Rudich, *Geophys. Res. Lett.*, 2001, **28**, 4083–4086.
23 U. Pöschl, T. Letzel, C. Schauer and R. Niessner, *J. Phys.Chem. A*, 2001, **105**, 4029–4041.
24 Y. Wadia, D. J. Tobias, R. Stafford and B. J. Finlayson-Pitts, *Langmuir*, 2000, **16**, 9321–9330.
25 A. K. Bertram, A. V. Ivanov, M. Hunter, L. T. Molina and M. J. Molina, *J. Phys. Chem. A*, 2001, **105**, 9415–9421.
26 M. J. Molina, A. V. Ivanov, S. Trakhtenberg and L. T. Molina, *Geophys. Res. Lett.*, 2004, **31**, L22104, DOI: 10.1029/2004gl020910.
27 Y. Dubowski, J. Vieceli, D. J. Tobias, A. Gomez, A. Lin, S. A. Nizkorodov, T. M. McIntire and B. J. Finlayson-Pitts, *J. Phys. Chem. A*, 2004, **108**, 10473–10485.
28 A. B. Voges, G. Y. Stokes, J. M. Gibbs-Davis, R. B. Lettan, P. A. Bertin, R. C. Pike, S. T. Nguyen, K. A. Scheidt and F. M. Geiger, *J. Phys. Chem. C*, 2007, **111**, 1567–1578.
29 J. Vieceli, O. L. Ma and D. J. Tobias, *J. Phys. Chem. A*, 2004, **108**, 5806–5814.
30 F. Karagulian, A. S. Lea, C. W. Dilbeck and B. J. Finlayson-Pitts, *Phys. Chem. Chem. Phys.*, 2008, **10**, 528–541.
31 T. M. McIntire, O. Ryder and B. J. Finlayson-Pitts, *J. Phys. Chem. C*, 2009, **113**, 11060–11065.
32 S. S. Cheng, D. A. Scherson and C. N. Sukenik, *J. Am. Chem. Soc.*, 1992, **114**, 5436–5437.
33 P. W. Hoffmann, M. Stelzle and J. F. Rabolt, *Langmuir*, 1997, **13**, 1877–1880.
34 I. C. Stefan and D. A. Scherson, *Langmuir*, 2000, **16**, 5945–5948.
35 S. Devouge, J. Conti, A. Goldsztein, E. Gosselin, A. Brans, M. Voué, J. De Coninck, F. Homblé, E. Goormaghtigh and J. Marchand-Brynaert, *J. Colloid Interface Sci.*, 2009, **332**, 408–415.
36 R. Maoz and J. Sagiv, *J. Colloid Interface Sci.*, 1984, **100**, 465–496.
37 J. M. Buriak, *Chem. Rev.*, 2002, **102**, 1271–1308.
38 J. G. Calvert and J. N. Pitts, Jr., *Photochemistry*, Wiley and Sons, Inc., 1966.
39 B. E. Ludwig and G. R. McMillan, *J. Am. Chem. Soc.*, 1969, **91**, 1085–1088.
40 A. Matsunaga and P. J. Ziemann, *J. Phys. Chem. A*, 2009, **113**, 599–606.
41 B. Pal and P. A. Ariya, *Environ. Sci. Technol.*, 2004, **38**, 5555–5566.
42 H. W. Thompson and F. S. Dainton, *Trans. Faraday Soc.*, 1937, **33**, 1546–1555.
43 J. Raff, personal communication, 2009.
44 N. J. Harrick, *Internal Reflection Spectroscopy*, Wiley Interscience Publishers, New York, 1967.
45 S. P. Sander, R. R. Friedl, D. M. Golden, M. J. Kurylo, G. K. Moorgat, H. Keller-Rudek, P. H. Wine, A. R. Ravishankara, C. E. Kolb, M. J. Molina, B. J. Finlayson-Pitts, R. E. Huie and V. L. Orkin, *Chemical Kinetics and Photochemical Data for Use in Atmospheric Studies JPL Publication 06-2*, NASA, 2006.
46 E. M. Pugh and G. H. Winslow, *The Analysis of Physical Measurements*, Addison-Wesley, Reading, MA, 1966.
47 D. L. Angst and G. W. Simmons, *Langmuir*, 1991, **7**, 2236–2242.
48 I. Engquist, I. Lundstrom and B. Liedberg, *J. Phys. Chem.*, 1995, **99**, 12257–12267.
49 J. Sagiv, *J. Am. Chem. Soc.*, 1980, **102**, 92–98.
50 Q. Zhang, Q. Zhang and L. A. Archer, *J. Phys. Chem. B*, 2006, **110**, 4924–4928.
51 S. G. Moussa, T. M. McIntire, M. Szori, M. Roeselova, D. J. Tobias, R. L. Grimm, J. C. Hemminger and B. J. Finlayson-Pitts, *J. Phys. Chem. A*, 2009, **113**, 2060–2069.
52 G. Socrates, *Infrared and Raman Characteristic Group Frequencies*, 3rd edn, John Wiley & Sons Ltd, 2001.
53 T. M. D'Andrea, X. Zhang, E. B. Jochnowitz, T. G. Lindeman, C. J. S. M. Simpson, D. E. David, T. J. Curtiss, J. R. Morris and G. B. Ellison, *J. Phys. Chem. B*, 2008, **112**, 535–544.
54 R. G. Nuzzo, L. H. Dubois and D. L. Allara, *J. Am. Chem. Soc.*, 1990, **112**, 558–569.
55 R. Banga, J. Yarwood, A. M. Morgan, B. Evans and J. Kells, *Langmuir*, 1995, **11**, 4393–4399.
56 M. Wang, K. M. Liechti, Q. Wang and J. M. White, *Langmuir*, 2005, **21**, 1848–1857.
57 S. Gross and A. K. Bertram, *J. Geophys. Res., [Atmos.]*, 2009, **114**, DOI: 10.1029/2008JD010987, Art. No. D02307.
58 R. Atkinson, *Atmos. Environ.*, 2007, **41**, 8468–8485.
59 A. Matsunaga, K. S. Docherty, Y. B. Lim and P. J. Ziemann, *Atmos. Environ.*, 2009, **43**, 1349–1357.
60 R. M. Garland, M. J. Elrod, K. Kincaid, M. R. Beaver, J. L. Jimenez and M. A. Tolbert, *Atmos. Environ.*, 2006, **40**, 6863–6878.
61 T. D. Klots and W. B. Collier, *Spectrochim. Acta, Part A*, 1994, **50**, 1725–1748.
62 G.-S. Wu, R. A. Stein and J. F. Mead, *Lipids*, 1977, **12**, 971–978.
63 G.-S. Wu, R. A. Stein and J. F. Mead, *Lipids*, 1978, **13**, 517–524.
64 K. U. Ingold, *Acc. Chem. Res.*, 1969, **2**, 1–9.
65 J. Arey, S. M. Aschmann, E. S. C. Kwok and R. Atkinson, *J. Phys. Chem. A*, 2001, **105**, 1020–1027.
66 J. Y. Zhang, T. Dransfield and N. M. Donahue, *J. Phys. Chem. A*, 2004, **108**, 9082–9095.
67 A. Vlasenko, I. J. George and J. P. D. Abbatt, *J. Phys. Chem. A*, 2008, **112**, 1552–1560.
68 T. M. McIntire, A. S. Lea, D. J. Gaspar, N. Jaitly, Y. Dubowski, Q. Q. Li and B. J. Finlayson-Pitts, *Phys. Chem. Chem. Phys.*, 2005, **7**, 3605–3609.
69 N. Winter, J. Vieceli and I. Benjamin, *J. Phys. Chem. B*, 2008, **112**, 227–231.
70 M. Szori, D. J. Tobias and M. Roeselova, *J. Phys. Chem. B*, 2009, **113**, 4161–4169.
71 R. L. Grimm, N. M. Barrentine, C. J. H. Knox and J. C. Hemminger, *J. Phys. Chem. C*, 2008, **112**, 890–894.
72 T. M. McIntire, O. S. Ryder, P. L. Gassman, Z. Zhu, S. Ghosal and B. J. Finlayson-Pitts, *Atmos. Environ.*, 2009, **44**, 939–944, DOI: 10.1016/jatmosenv.2009.1011.1009, available online.
73 K. S. Docherty and P. J. Ziemann, *J. Phys. Chem. A*, 2006, **110**, 3567–3577.
74 J. D. Hearn, L. H. Renbaum, X. Wang and G. D. Smith, *Phys. Chem. Chem. Phys.*, 2007, **9**, 4803–4813.
75 P. A. J. Bagot, C. Waring, M. L. Costen and K. G. McKendrick, *J. Phys. Chem. C*, 2008, **112**, 10868–10877.
76 I. J. George, A. Vlasenko, J. G. Slowik, K. Broekhuizen and J. P. D. Abbatt, *Atmos. Chem. Phys.*, 2007, **7**, 4187–4201.
77 J. D. Hearn and G. D. Smith, *Geophys. Res. Lett.*, 2006, **33**, L17805, DOI: 10.1029/2006gl026963.
78 A. T. Lambe, J. Zhang, A. M. Sage and N. M. Donahue, *Environ. Sci. Technol.*, 2007, **41**, 2357–2363.
79 V. F. McNeill, G. M. Wolfe and J. A. Thornton, *J. Phys. Chem. A*, 2007, **111**, 1073–1083.
80 V. F. McNeill, R. L. N. Yatavelli, J. A. Thornton, C. B. Stipe and O. Landgrebe, *Atmos. Chem. Phys.*, 2008, **8**, 5465–5476.
81 J. D. Smith, J. H. Kroll, C. D. Cappa, D. L. Che, C. L. Liu, M. Ahmed, S. R. Leone, D. R. Worsnop and K. R. Wilson, *Atmos. Chem. Phys.*, 2009, **9**, 3209–3222.
82 E. A. Weitkamp, A. T. Lambe, N. M. Donahue and A. L. Robinson, *Environ. Sci. Technol.*, 2008, **42**, 7950–7956.

